Fluctuations in the ^{235}U(n, f) cross section

G. F. Bertsch, David Brown, and E. D. Davis

Phys. Rev. C **98**, 014611 — Published 18 July 2018

DOI: 10.1103/PhysRevC.98.014611

Fluctuations in the ^{235}U(n,f) cross section

G.F. Bertsch

Department of Physics and Institute of Nuclear Theory, Box 351560

*University of Washington, Seattle, Washington 98915, USA**

David Brown

National Nuclear Data Center, Brookhaven National laboratory, Upton NY, USA†

E.D. Davis

Department of Physics, North Carolina State University,

Raleigh, North Carolina 27695-8202, USA and

Triangle Universities Nuclear Laboratory,

Durham, North Carolina 27708-0308, USA‡

Abstract

We examine the autocorrelation function of the ^{235}U(n,f) reaction with a view to quantify the presence of intermediate structure in the cross section. Fluctuations due to compound nucleus resonances on the eV energy scale are clearly visible up to ≈ 100 keV neutron energies. Structure on the one-keV energy scale is not present as a systematic feature of the correlation function, although it is present in the data covering the region around 20 keV.

* bertsch@uw.edu

† dbrown@bnl.gov

‡ dedavis4@ncsu.edu

I. INTRODUCTION

The fluctuations in reaction cross sections convey important information about the reaction dynamics. Low-energy reactions on heavy nuclei are typically described by the Hauser-Feshbach extension of Bohr's compound nucleus model, and contain as parameters the density of the compound nucleus resonances and the effective number of channels participating in the reaction. When the properties of the resonances cannot be individually measured, one relies on a fluctuation analysis such as we use below to gain information about their properties. Understanding the neutron-induced fission reaction is even more challenging because there is no reason to believe that a simple compound nucleus picture is adequate to deal with the large-amplitude shape changes the excited nucleus undergoes. This gives a strong motivation to characterize as quantitatively as possible the fluctuations associated with the reaction, in order to better understand the reaction dynamics.

Part of the complexity of the reaction is due to the presence of multiple fission barriers. At energies below the barriers, the cross section can fluctuate due to resonant states located between the barriers. Above the barriers, the situation remains unclear. There is evidence for structure on the keV energy scale from experiments carried out in the 1970's on the ^{235}U(n,f) reaction with neutron energies in the range 1–100 keV. The compound nucleus energies exceed the barrier top by ≈ 1 MeV, so below-barrier resonances could not be the cause. Many experimental measurements have been made encompassing that energy range, as detailed in Appendix A. Three of them have the resolution and documentation to make a case for the presence of fluctuations on a keV energy scale. Their measured cross sections between 10 and 25 keV are shown in Fig. 1. All three show a clear peak at 22 keV, having a width about 1 keV. There may be correlated peaking at lower energies as well. The abstract of one of the papers (Ref. [1]) states: "The previously reported intermediate structure in the fission cross section in the keV region is confirmed by the results of this work." Nevertheless, such structures have not be documented as a general feature of cross sections at energies above the barrier. The aim of this work is to analyze the cross section fluctuations in a systematic way to see if quantitative information about them can be extracted.

Our analysis tool is the autocorrelation function R defined as [4, 5]

$$R(\varepsilon) = \left\langle \frac{(\sigma(E_+) - \bar{\sigma}(E_+))(\sigma(E_-) - \bar{\sigma}(E_-))}{\bar{\sigma}(E_+)\bar{\sigma}(E_-)} \right\rangle \tag{1}$$

where $E_\pm = E \pm \varepsilon/2$. The angle brackets denote an average over the energy E and $\bar{\sigma}$ is

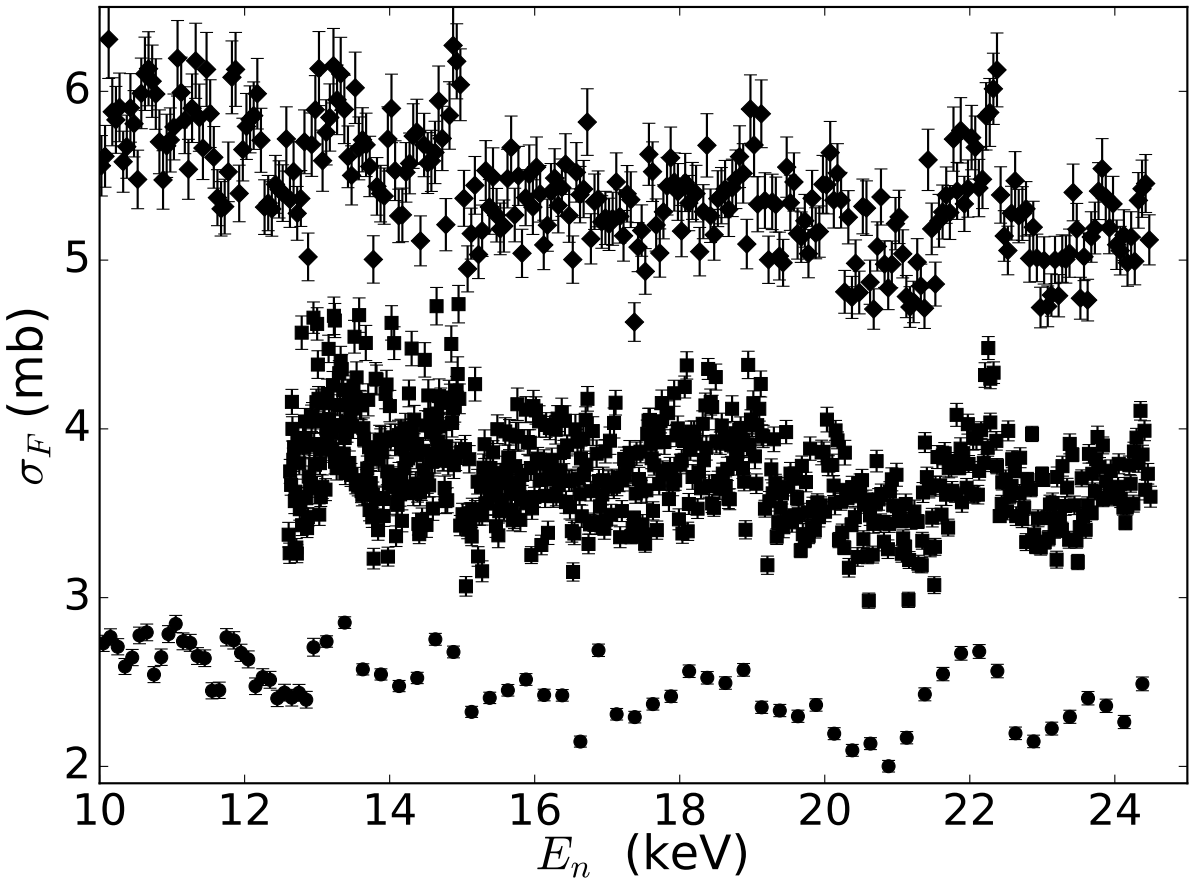

FIG. 1. Experimental fission cross sections in the range 10 - 25 keV. Circles: from Ref. [2]; squares: from [3]; diamonds: from [1]. The latter two data sets have been shifted upward for clarity in the plotting of the figure.

an energy-dependent averaged cross section, with the details to be specified later. To keep the number of entrance channels to a minimum, we limit the analysis to neutron energies below 100 keV, which is sufficient to span the structure of interest at 22 keV. The analysis of cross section fluctuations by the autocorrelation function has a long history in nuclear physics, starting from Ericson's analysis [6, 7] aimed at conditions where the resonances are strongly overlapping. See Ref. [8] for an early review. Other methods have been proposed as well. One analysis is based on the Fourier transform of the energy variable to the time domain [8, pp. 372-373]. Another method is based on counting peaks in the cross section [9–11], recently applied in Ref. [12].

The organization of this article is as follows. In Section II, we review the interpretation

of the autocorrelation function and its parameterization. In Section III, we confirm the expected behavior of the autocorrelation function in the isolated-resonance region at the lowest energies. The data in the higher energy region of unresolved resonances is analyzed in Sect. IV. Section V summarizes the two main conclusions of our analysis. The first conclusion is that the eV-scale correlations due to compound nucleus resonances are present and affect the correlation function far beyond the isolated resonance region. Second, only a limit can be placed on any systematic correlation structure at the one-keV energy scale. Thus the peaking seen in Fig. 1 is an isolated feature of the energy-dependent cross section. We argue for a campaign of new measurements to pinpoint the origin of the observed structure and to see if it occurs in above-barrier fission of other nuclei.

II. THE AUTOCORRELATION FUNCTION

Before discussing practical details of calculating and interpreting cross section fluctuations, we review the analytic statistical theory of the autocorrelation function $C(\varepsilon)$. It is defined

$$C(\varepsilon) = \overline{\left(\sigma(E_+) - \overline{\sigma}\right)\left(\sigma(E_-) - \overline{\sigma}\right)} \Big/ \overline{\sigma}^2 \; . \tag{2}$$

Here the overline denotes an average over an ensemble of S-matrix elements that enter the cross sections, Eq. (3) below. The ensemble is generated from a statistical model of compound nucleus resonances. The ensemble averages are calculated at fixed energy, but by construction they do not depend on that energy. It is implicitly assumed that the energy averaging in $R(\varepsilon)$ is equivalent to the ensemble averaging in $C(\varepsilon)$.

The first step in calculating $C(\varepsilon)$ is to express the cross sections in terms of their S-matrix elements,

$$\sigma = \frac{\pi}{k_n^2} \sum_{i,c} g^J |S_{ic}|^2. \tag{3}$$

Here i denotes the quantum numbers specifying an incident (s-wave) neutron channel of angular momentum J and parity π, c denotes the quantum numbers of an exit fission channel (of the same J^π), and g^J is the usual spin statistical factor. $C(\varepsilon)$ can then be written as the incoherent superposition

$$C(\epsilon) = \sum_{i,c,c'} w_{ic} w_{ic'} C_{icc'}(\epsilon), \tag{4}$$

of the autocorrelation functions for each channel i,

$$C_{icc'}(\varepsilon) = \frac{\overline{|S_{ic}(E+\epsilon/2)|^2 |S_{ic'}(E-\epsilon/2)|^2} - \overline{|S_{ic}|^2}\ \overline{|S_{ic'}|^2}}{\overline{|S_{ic}|^2}\ \overline{|S_{ic'}|^2}} \tag{5}$$

together with the weighting factors

$$w_{ic} = \frac{g^J\ \overline{|S_{ic}|^2}}{\sum\limits_{i,c'} g^J \overline{|S_{ic'}|^2}}. \tag{6}$$

The correlations of interest are determined by the $C_{icc'}$, but their amplitude in $C(\varepsilon)$ depends on the number of fission channels and other information carried by the weights.

We will see later that the ε- and w_{ic}-dependence are easy to disentangle in the isolated resonance regime, as well as the regime with strongly overlapping resonances.

A. The statistical Breit-Wigner model

Our derivation of $C_{icc'}(\varepsilon)$ proceeds by modeling the S-matrix by a sum of Breit-Wigner resonances,

$$S_{ab}(E) = \delta_{ab} - i \sum_k \frac{\gamma_{ak}\gamma_{kb}}{E - e_k}. \tag{7}$$

The poles are at complex energies $e_k = E_k - i\Gamma_k/2$, where the widths Γ_k are related to the real-valued partial width amplitudes γ_{ck} by $\Gamma_k = \sum_c \gamma_{ck}^2$. Evaluation of Eq. (5) requires assumptions about the distribution and correlations of γ_{ck} and E_k. Here we are guided by the empirical success of the Gaussian Orthogonal Ensemble (GOE) of Hamiltonian matrices. According to the GOE model, partial width amplitudes γ_{ak} are distributed for different resonances k as a Gaussian random variable of zero mean; the corresponding variance depends on the choice of channel a alone. Furthermore, partial width amplitudes relating to different open channels a are completely uncorrelated. As a consequence, for inelastic processes ($a \neq b$), the ensemble average of S_{ab} in Eq. (7) yields $\overline{S_{ab}} = 0$.

Our treatment of the e_k in the energy denominator deviates from a strict application of GOE level correlation statistics. Instead of using Dyson's celebrated result for the two-level cluster function Y_2 [13], we follow Ref. [14] and adopt the simplified but effective parameterization

$$Y_2(\Delta E/\bar{D}) \approx \frac{1}{1 + (\pi \Delta E/\bar{D})^2} \tag{8}$$

where ΔE is the difference of two resonance energies of the same spin and parity, and $\bar{D}$ is the average level spacing for that spin and parity. The imaginary part of e_k, namely $\Gamma_k/2$ is assumed to be constant. Neglect of fluctuations in the *total* widths Γ_k will be a source of inaccuracy if there are only a few open fission channels. (We return to this point below.)

Note that the analysis of the ensemble is at a fixed energy and thus not able to deal with secular variations of the parameters with respect to energy. Thus the theory does not address effects related to penetrability factors in the amplitudes γ_{ak} or to increase of level densities with excitation energy.

B. Analytic approximations for $C_{icc'}(\varepsilon)$

Compact integral representations of the averages in $C_{icc'}(\varepsilon)$ can be derived using the method presented in Ref. [14]. Our replacement of the different total widths Γ_k by a single total width Γ permits us to infer explicit expressions which capture many of the essential features of $C_{icc'}(\varepsilon)$. In terms of the ratio $x = \bar{D}/\pi\Gamma$, our full result for $C_{icc'}(\varepsilon)$ reads

$$\begin{aligned} C_{icc'}(\varepsilon) \approx 3(1+2\delta_{c,c'})&\frac{x\Gamma^2}{\varepsilon^2+\Gamma^2} \\ &- \left(\frac{x}{x+1}\right)\frac{\Gamma^2}{\varepsilon^2+\Gamma^2} - \frac{x(x+1)\Gamma^2}{\varepsilon^2+(x+1)^2\Gamma^2} \\ &- \left(\frac{x}{x+1}\right)\frac{\Gamma^2}{\varepsilon^2+(x+1)^2\Gamma^2} \\ &+ \delta_{c,c'}\frac{\Gamma^2}{\varepsilon^2+\Gamma^2}. \end{aligned} \tag{9}$$

In the limit $\varepsilon = 0$ and $c = c'$, Eq. (9) reduces to the second line of Eq. (B12) in Ref. [14], when allowance is made for the different grouping of terms, the identification of Γ with the Weisskopf estimate Γ_W for the correlation width, and a typographical error[1].

The four lines in Eq. (9) correspond to three physically distinct contributions to $C_{icc'}(\varepsilon)$: on the first line, a resonance self-correlation piece, dominant when $\bar{D} \gg \Gamma$ (isolated resonance regime); on the second and third lines, negative terms arising from level repulsion correlations between pairs of distinct resonances, and; finally, on the fourth line, a cross section auto-correlation function of the kind derived by Ericson [6], dominant when $\bar{D} \ll \Gamma$, i.e., in the strongly overlapping resonance regime.

[1] A plus sign should precede the "1" at the end of the second line of Eq. (B12) in Ref. [14].

In the limit of large or small x, Eq. (9) depends on ε only by an overall factor $\Gamma^2/(\varepsilon^2+\Gamma^2)$. In Appendix V B we show that the factorization can be extended over the entire range of x with only a slight degradation of accuracy with the formula

$$C_{icc'}(\varepsilon) \approx C_{icc'}(0)\frac{\Gamma^2}{\varepsilon^2+\Gamma^2}, \tag{10}$$

where

$$C_{icc'}(0) \approx \Big[(1+6x)\delta_{cc'} + (3x-1)\Theta(3x-1)\Big] \tag{11}$$

and $\Theta(x)$ is the Heaviside step function.

With the above approximations, it is easy to carry out the sum of c and c' in Eq. (4). $C(\varepsilon)$ has the form

$$C(\varepsilon) = C(0)\frac{\Gamma^2}{\varepsilon^2+\Gamma^2} \tag{12}$$

where

$$C(0) \approx (1+6x)\sum_{i,c} w_{ic}^2 + (3x-1)\Theta(3x-1)\sum_{i,c,c'} w_{ic}w_{ic'}, \tag{13}$$

Note that the two sums depend on the number of significant entrance and exit channels. The sum $\sum_{i,c} w_{ic}^2$ in the first term of Eq. (13) appears in the theory for strongly overlapping resonances [5, 7, 15, 16] as the damping factor N^{-1}. However, Eq. (13) applies to a broader range of conditions than the formulas derived in these publications.

C. Extracting R from experimental data

Several compromises must be made to apply Eq. (1) and interpret the results. For the data treated here in detail, the experimental cross sections are provided as average cross sections on a mesh of energies with mesh spacing ΔE covering some range of energy $[E_0 - B/2, E_0 + B/2]$. The cross sections are given as a list σ_n where n specifies the energy $E_n = E_0 - B/2 + n\Delta E$. The ratio in Eq. (1) is computed for each pair of cross sections in the list, and a running sum $\Sigma(|n-n'|)$ is kept for each energy difference $E_n - E_{n'}$. The computed autocorrelation function is $R(\varepsilon) = \langle\Sigma(m)\rangle$ where the angular brackets denote the average for that bin.

In the analysis presented below, we define a local average cross section $\langle\sigma(E)\rangle_l$ by making a linear fit

$$\langle\sigma(E)\rangle_l = \sigma_0 + b(E-E_0) \tag{14}$$

to the data in the interval. We have also analyzed some of the data with a quadratic fit and found that the extracted correlation is hardly changed. One can develop a semi-analytic justification based on the assumption that the actual variation of the local average cross section is due to the s-wave penetrability factor, giving $\langle\sigma(E)\rangle_l \approx E^{-1/2}$. With our bandwidths B, which are such that $B/E_0 < 1$, a linear fit produces an error of less than 1% in $R(0)$.

The analysis will show a peak at $\epsilon = 0$ which may or may not extend to other bins. The experimental statistics are not good enough to test the actual shape of peak, but we can extract $R(0)$ and some measure of the peak width within the experimental uncertainty limits of the data. We shall extract an "experimental" Γ as the value of ε satisfying $R(\varepsilon) = R(0)/2$.

Equation (12) does not take into account the finite energy resolution of an experimental measurement. Typically, cross sections are reported as averages over energy bins ΔE. The effect on $R(\varepsilon)$ is analyzed in Appendix C. In the limit $\varepsilon \gg \Delta E$ the peak occurs only in the first bin, and its height $R_{\Delta E}$ is

$$R_{\Delta E} \approx R(0)\frac{\pi\Gamma}{\Delta E}. \tag{15}$$

Equation (15) applies to the data sets we consider in section IV as these involve multi-keV neutron energies, for which the experimental resolution is much broader than the widths of the compound-nucleus states.

III. RESOLVED RESONANCE REGION

As a warm-up to the computation of R on multi-keV energy intervals, we consider fluctuations in the resolved resonance region below 100 eV. Figure 2 shows the experimental cross section for the neutron energy range 10–30 eV, with the data taken from the ENDF-VIII.0 evaluated cross section [17–19][2]. The corresponding autocorrelation function calculated from Eq. (1) is shown in Fig. 3. There is a clear peak at $\varepsilon = 0$. Its shape parameters are $R(0) = 4.23$ and $\Gamma_{HM} = 0.09$ eV. Table II gives the peak parameters as well as those for other energy ranges below 100 eV. Both $R(0)$ and Γ_{HW} change with increasing energy E. There is also a prominent peak at $\varepsilon = 7$ eV, which we interpret as a statistical fluctuation of no physical significance.

[2] The ENDF evaluation also has individual resonance parameters, but we also use the reconstructed cross section to extract the autocorrelation function.

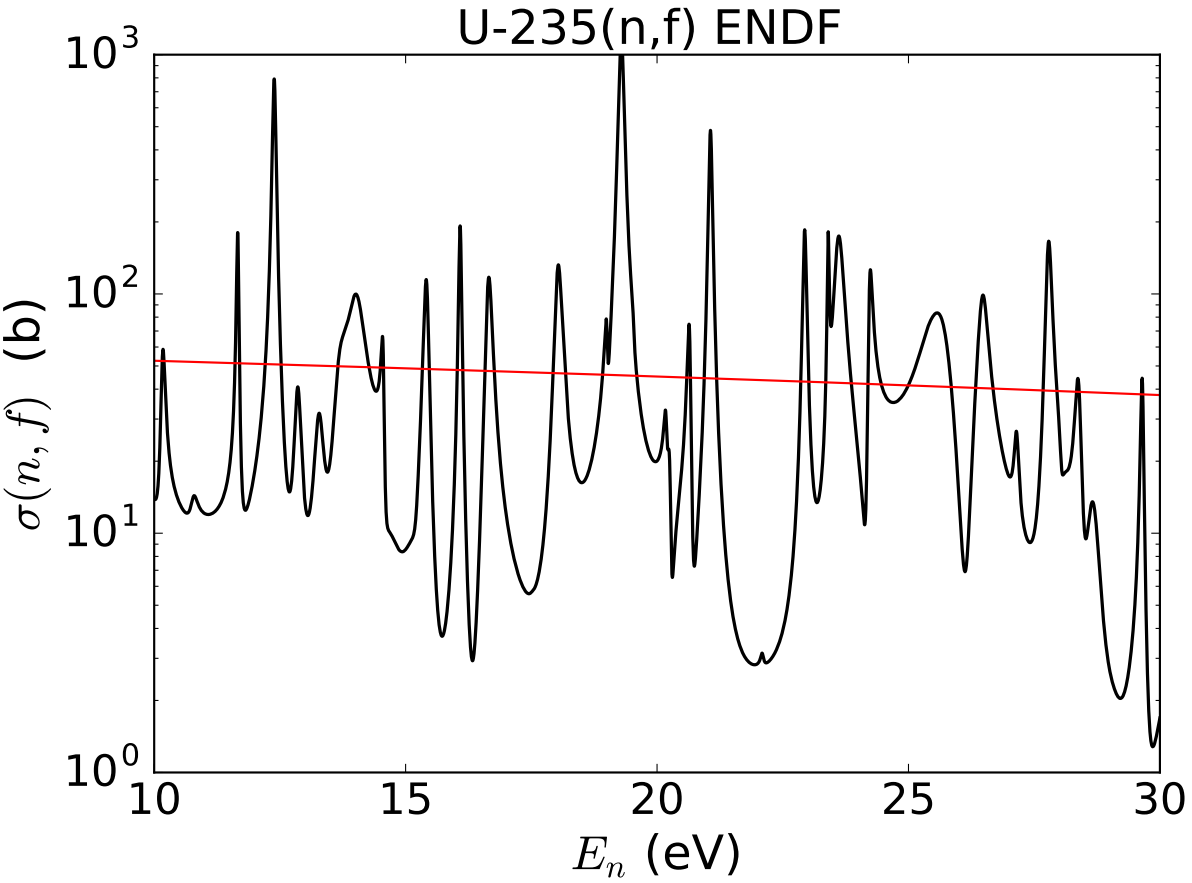

FIG. 2. ^{235}U(n,f) cross section from the ENDF/VIII.0 database. The red line shows the fitted average cross section, $\bar{\sigma} = 45.2 - 0.74(E_n - 20\text{ eV})$ b. See Supplementary Material [20] for the scripts used to produce the data for this Figure and for Figs. 3-6.

To see how well one can understand the peak at $\varepsilon = 0$, we first compare with the prediction of the analytic model, Eq. (9). The reaction parameters for one entrance channel are given in Table II [3]. The total width Γ is the sum of the width in the entrance channel Γ_n, the capture width Γ_γ, and the fission width Γ_f. The fission width be computed from the parameters in Table II as $\Gamma_f \approx \alpha^{-1}\Gamma_\gamma = 0.064$ eV. The entrance-channel width is computed as $\Gamma_n \approx S_0 E^{-1/2}\pi/k_n^2$, where k_n is the neutron momentum in the entrance channel. It is entirely negligible compared to $\Gamma_f + \Gamma_\gamma$ for energies under 1 keV. Thus, $\Gamma \approx \Gamma_\gamma + \Gamma_f = 0.102$ eV over the region covered in Table I. This yields $x = 0.94/(0.102\pi) = 2.9$. We also need the number of channels and their weights to apply Eq. 13. There are two entrance channels in

[3] Note that $D = 0.47$ includes resonances from both entrance channels ($J^\pi = 3^-$ and 4^-).

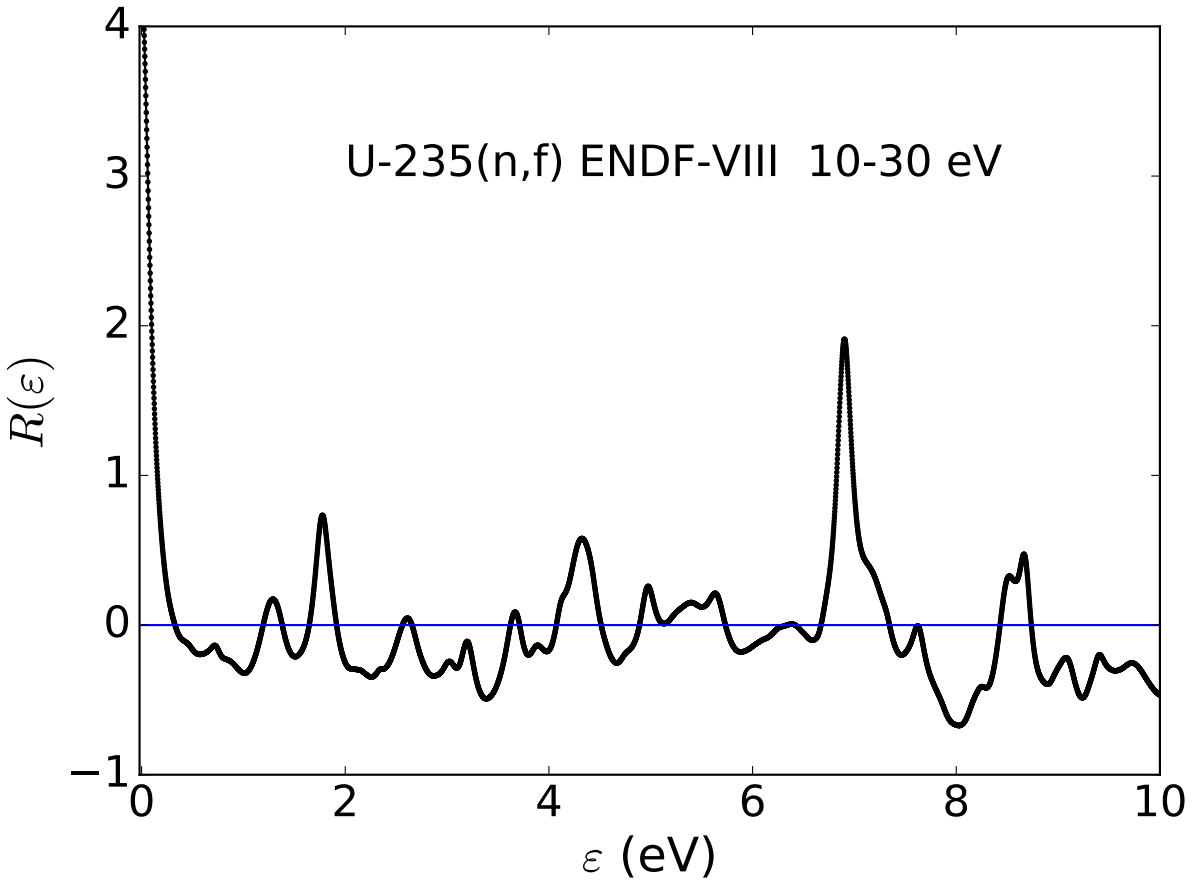

FIG. 3. Autocorrelation $R(\varepsilon)$ for the data shown in Fig. 2 for the range $0 < \varepsilon < B/2$.

the ^{235}U(n,f) reaction at low energy, namely $J = 3$ and $J = 4$, and it is reasonable to assume that their weights are close to equal. The situation is less clear for the fission channels. Very likely there are only a few channels that contribute strongly. Let us assume that there are three fission exit channels for each entrance channel, and they all contribute equally. Then the weighting factors in Eq. 13 are $\sum_{i,c} w_{ic}^2 = 1/6$ and $\sum_{i,c,c'} w_{ic} w_{ic'} = 1/2$. Inserting these numbers in Eq. 13 we find $R(0) \approx 7.0$. This overestimate arises because of our neglect of fluctuations in the total fission width, which can be sizable if there are only three channels. These effects are included in the equations derived in Ref. [14], but evaluating them requires several numerical integrations and are not easy to condense to a simple formula. Apart from that, the observed variation of $R(0)$ over the 100 eV energy range of data set is inexplicable. None of the compound nucleus parameters vary significantly on such a small energy scale, and the entrance channels widths are small over the entire range.

	ENDF			Mazama		
Energy range	σ_0(b)	$R(0)$	Γ_{HM}(eV)	σ_0(b)	$R(0)$	Γ_{HM}(eV)
10 - 30 eV	45.2	4.23	0.09	51 ± 13	3.6 ± 1.4	0.10 ± 0.02
30 -50	44.7	2.58	0.10			
50 -70	37.	2.40	0.16			
70 -90	29.9	1.42	0.17	27 ± 6	3.2 ± 1.0	0.10 ± 0.02

TABLE I. Autocorrelation peak height and width for various energy ranges. The Mazama program and the scripts for the entries on line 1 are included in the Supplementary Material [20].

parameter	value	source
$D = \bar{D}/2$	0.47 eV	[17]
$\bar{\Gamma}_\gamma$	0.038 eV	[17]
S_0	0.98×10^{-4} eV$^{-1/2}$	[17]
α^{-1}	1.69	[21]

TABLE II. Reaction parameters for the neutron reactions on ^{235}U at low energy. The parameter $\alpha^{-1} = \langle\sigma(n,f)\rangle/\langle\sigma(n,\gamma)\rangle$ is evaluated taking the averages over the energy range $E_n = 10$–100 eV.

The correlation widths should be equal to the total widths of the compound nucleus resonances in the isolated resonance regime. This appears to be the case for the first two energy ranges in Table I, taking Γ from the paragraph above. However, the extracted experimental width increases in the higher energy ranges. Again, this is not explicable given our understanding of how the compound nucleus parameters vary with energy.

One of us (GFB) has produced a Hamiltonian model that includes both a GOE treatment of the resonances and an explicit Hamiltonian treatment of the entrance channel. The code, called "Mazama", is briefly described in the Appendix together with the Hamiltonian parameters as applied to this work. All the fluctuations inherent in the GOE are included, since the code operates by sampling the ensemble and calculating the full energy-dependent cross section for each representative Hamiltonian. The parameters of the ensemble are tuned to reproduce the experimental D, Γ_γ and α^{-1}. The number of fission channels is taken to be 3. A typical cross section produced by Mazama is shown in Fig. 4. The calculation was

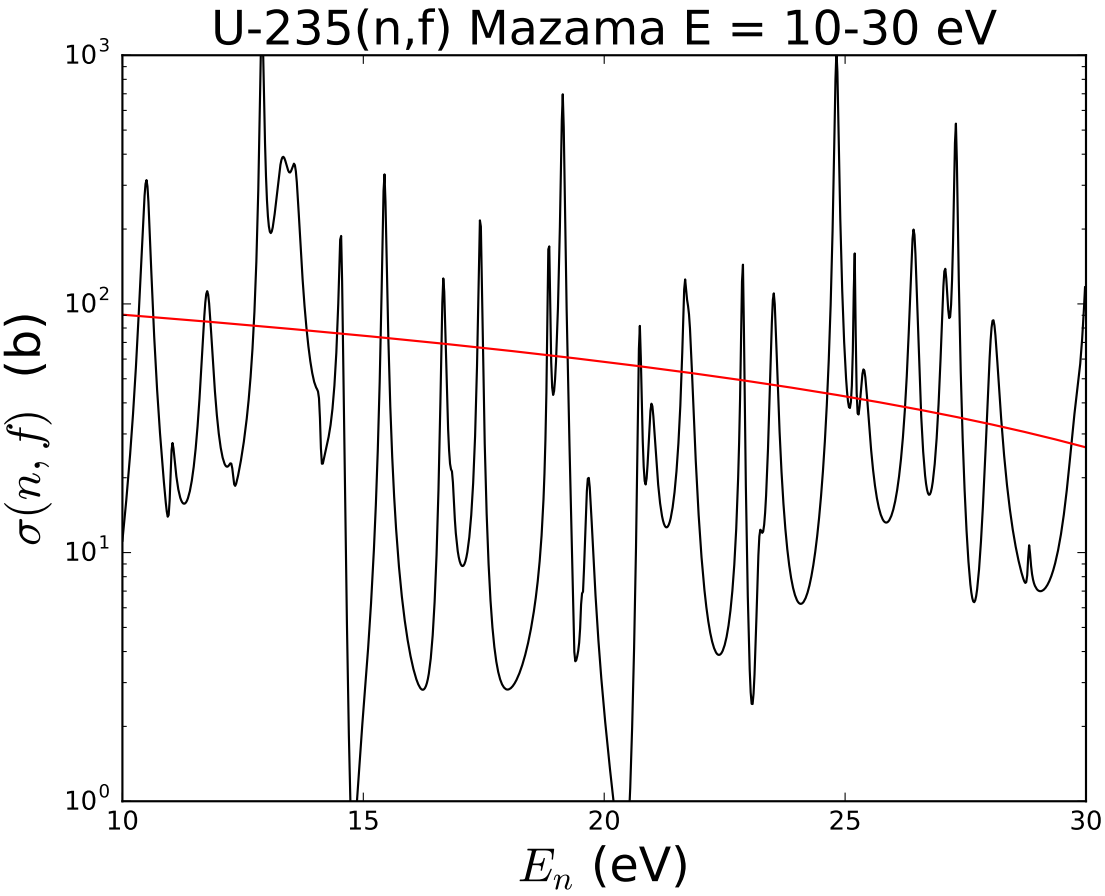

FIG. 4. Sample ^{235}U(n,f) cross section calculated by the mazama code. The results are the average for two entrance channels. Code parameters are given in the Appendix.

done by taking two samples from the ensemble, for the two independent entrance channels. The extracted autocorrelation function is shown in Fig. 5. The related peak parameters are $R(0) = 4.1$ and $\Gamma_{HM} = 0.08$ eV, in fair agreement with the ENDF data shown in Figs. 2 and 3. Of course there are uncertainties in the predicted peak parameters due to the Porter-Thomas fluctuations. These can be estimated by taking many samples from the GOE ensemble, evaluating the parameters for each sample, and then finding the rms dispersion in them.

We have carried out this analysis for 100 samples to determine a mean and dispersion of the parameters. The results are given in the leftmost columns of Table I. The error bars on the extracted quantities are the standard deviations of the individual samples. The ensemble averages for the 10–30 eV interval agree with the experimental numbers for the

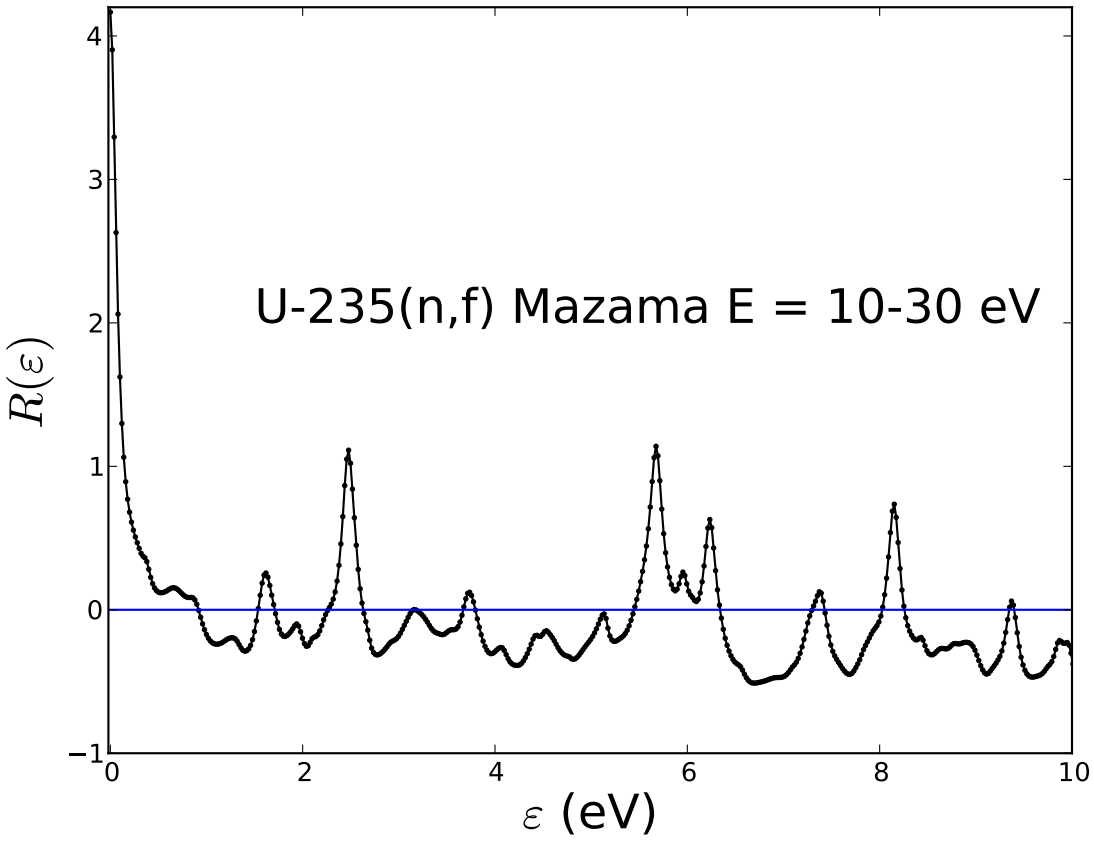

FIG. 5. Autocorrelation $R(\varepsilon)$ for the data shown in Fig. 4.

cross section and $R(0)$ value to within the error bars. The Mazama analysis confirms that the GOE model has the potential to describe data on $R(0)$.

The GOE model also shows that the uncertainty in the extracted $R(0)$ can be uncomfortably large. The variance in the calculated $R(0)$ is in the 30–40 % range with about 40 resonances in the energy window $B = 20$ eV. Assuming that standard statistics applies for errors, we estimate that the window should include about 500 resonances to reduce the uncertainty in $R(0)$ to the 10% level.

One can also see from Mazama model results for the 70–90 eV interval that the theoretical quantities hardly vary at all from those of the 10–30 eV interval. This is not unexpected, since the only real difference is the increased penetrability in the entrance channel. This substantiates our earlier assertion that the strong energy dependence of the $R(0)$ and Γ_{HM} obtained from ENDF cross sections is completely inexplicable in standard models of com-

pound nucleus reactions. However, for the purpose of our subsequent discussion of cross section fluctuations at multi-keV energies, we shall take the point of view that, as regards the 10–30 eV data and its modeling by the Mazama code, a good account is given of the primary peak in R. It is unambiguously associated with fluctuations in properties of individual compound-nucleus resonances.

IV. HIGHER ENERGY REGION

We now go to the multi-keV energy region where evidence for fluctuations on the keV energy scale were reported. We focus on the experimental data in Ref. [1] which covers the energy range 2–100 keV. The autocorrelation is computed in energy windows ranging in size from 3 keV to 20 keV. It is safe to assume that the resonance spacing D in this higher-energy region is unchanged from its value at energies below 100 eV. Then there are 3000 to 40,000 resonances in the window, giving adequate statistics for calculating $R(0)$. The bin size in the data is $\Delta E = 0.05$ keV, and the autocorrelation function is computed with the same binning. For each window, the average cross section is fitted to Eq. (14) for the data in that window. The error bars on $R(\varepsilon)$ are determined from an ensemble of data sets. The members are generated by adding a random error to the measured ones, with variance of the added error taken to be the quoted error of the tabulated experimental data. From the ensemble of computed $R(\varepsilon)$ values we report the mean and variance.

The results are shown in Fig. 6. One sees a spike in the bin at $\varepsilon = 0$, but hardly any structure beyond that. The corresponding $R(0)$ values are plotted in Fig. 7. Since the bin size is much larger than the compound nucleus resonance width, we expect Eq. (15) to apply to the $R(0)$ enhancement over the nearby ε bins.

With the given D and ΔE, Eq. (15) gives $R(0) \approx 0.022$, indicated in the Figure by the dashed line. The experimental $R(0)$ agrees with the expectation for the two lowest energy windows, but but it falls short at higher energy. A possible explanation is the finite energy resolution of measurements. If the resolution is of the order of the bin size, the $R(0)$ peak will spill out into neighboring bins. For example, $R(\varepsilon)$ for the 70-90 keV window is significantly above the axis for all the bins up to $\varepsilon = 0.25$ keV. Assuming that the cause is a spill-out, we should recover the original $R(0)$ by summing over these bins. The summed value is shown as the square symbol in Fig. 7. The agreement with the expected value is good enough to

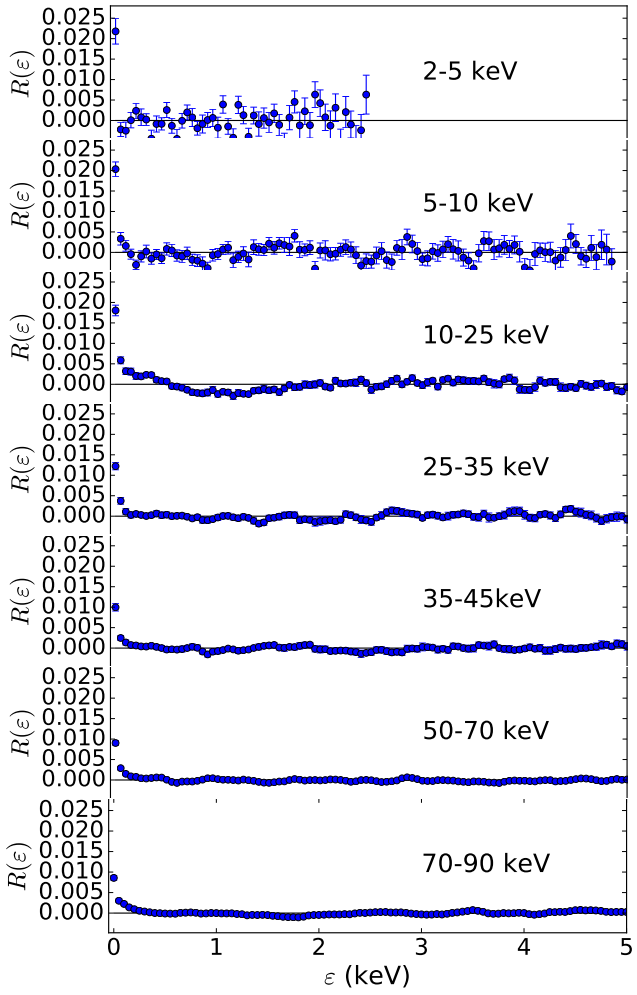

FIG. 6. Autocorrelation function for the ^{235}U(n,f) reaction over the energy range $2 < E < 90$ keV, using the cross section data of Ref. [1] as given in Ref. [21].

ascribe the finite-width suppression to spill-out rather than new physics.

The 10-25 keV energy window shown in Fig. 6 is exceptional: there is a peak at small ε that has no simple explanation. Fig. 8 shows the autocorrelation function with an expanded vertical scale. Besides the presence of a finite-width peak beyond the $R(0)$, the autocorrelation function becomes negative around $\varepsilon \approx 1$ keV. Theoretically, the autocorrelation function in Eq. (9) can be negative due to the repulsion between levels in the GOE. However, this is a very mild effect and the compound-nucleus resonances would only affect $R(\varepsilon)$ on a 1 eV energy scale.

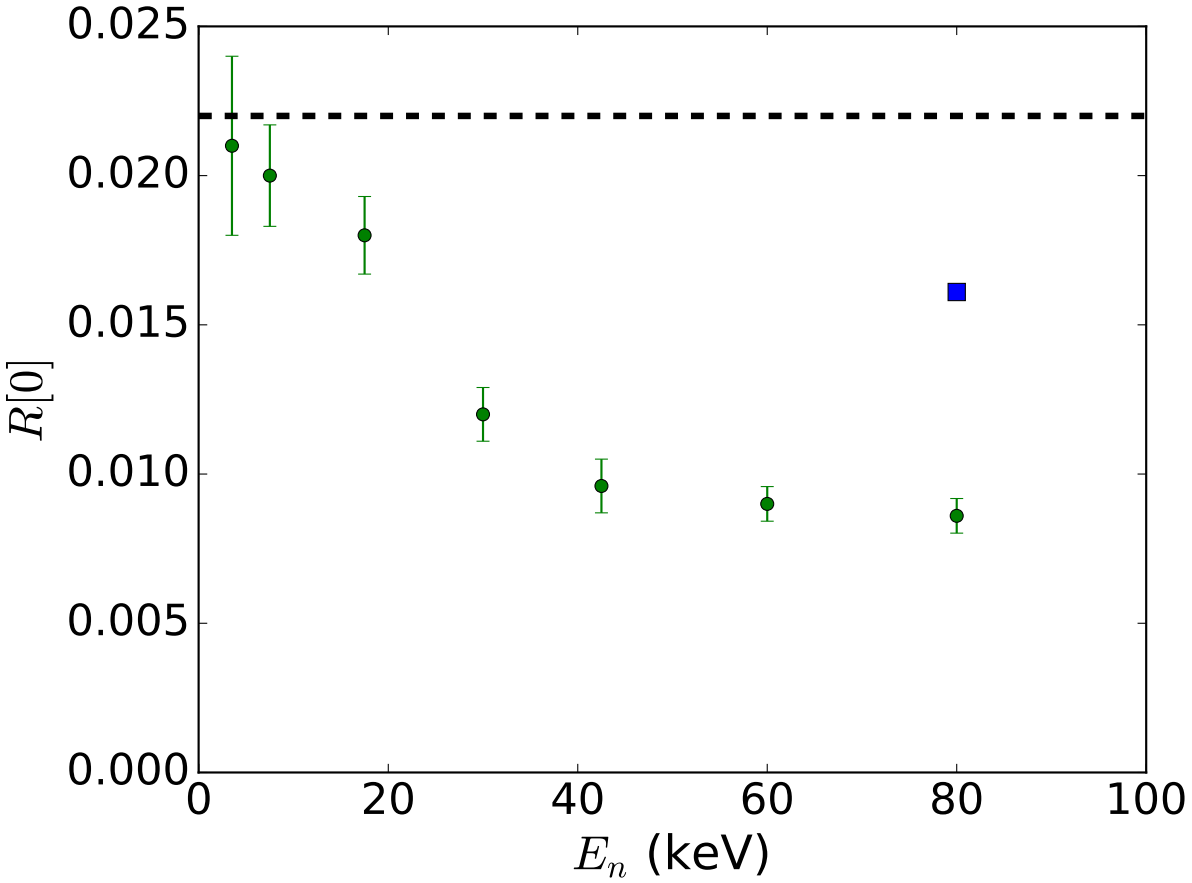

FIG. 7. Autocorrelation spike for the data of Ref. [1], showing several energy windows, beginning with 2–5 keV and ending with 70–90 keV. Error bars are computed from the quoted experimental errors in the data. The dashed line shows the value expected from the compound-nucleus resonance fluctuations. The blue square shows the reconstructed value for the 70–90 keV window as described in the text.

V. CONCLUSION AND OUTLOOK

While we confirm the effect of compound-resonances on the autocorrelation function up to near 100 keV in neutron bombarding energy, we see no evidence for correlations on the scale of 1 keV, contrary to the claim of Ref. [1]. Indeed, the only structure we observe is isolated in the 10-25 keV energy window.

Neutron-induced fission is very different below the barrier. There states in the second well mediate barrier penetration producing broad resonances in the fission cross sections.

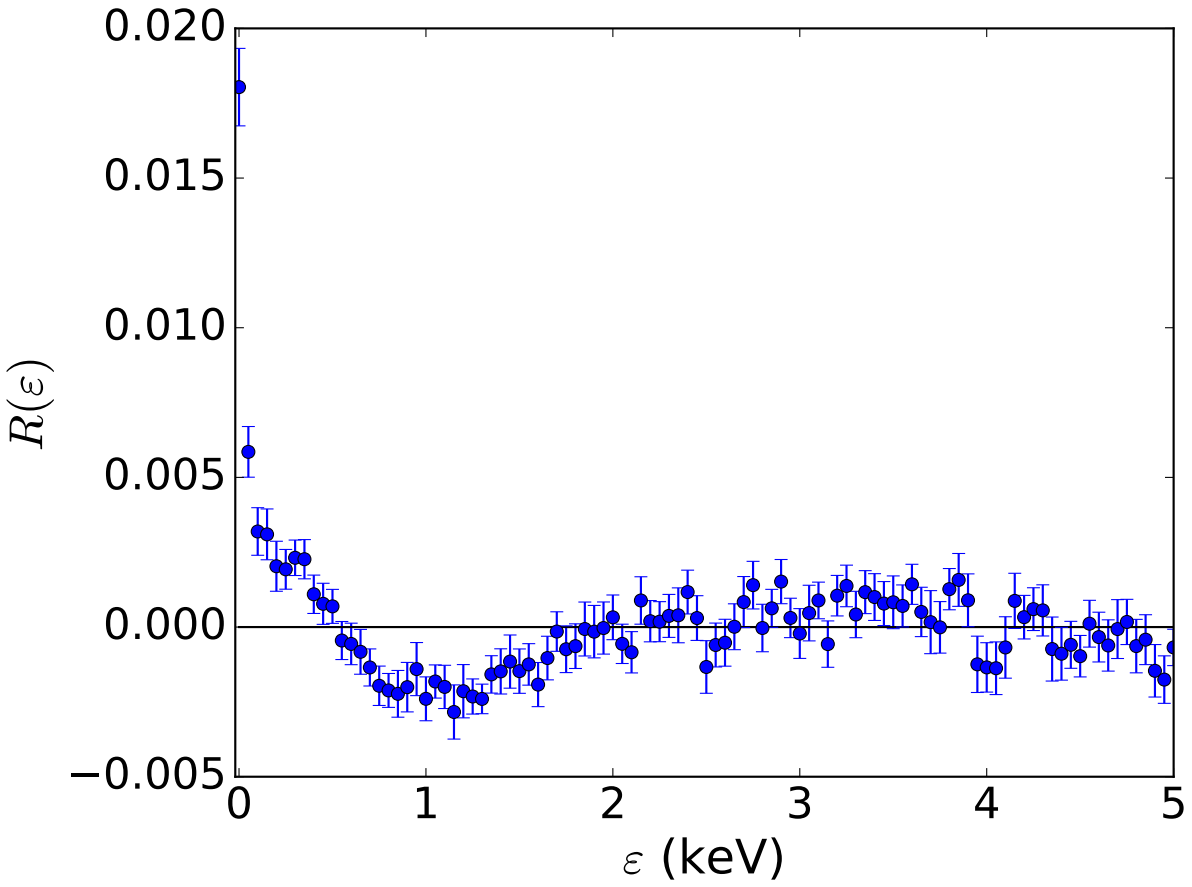

FIG. 8. Autocorrelation function for the ^{235}U(n,f) reaction over the energy range $10 < E < 25$ keV, using the cross section data of Ref. [1] as given in Ref. [21].

It might be that these resonances persist above the barrier in an attenuated form. That could be a plausible explanation of the 22 keV structure, provided the resonance spacing in the second well is compatible with the non-observation of other structure in the 2–100 keV energy range. Perhaps more experimental study of fission cross sections around the barrier top would clarify the situation. In that respect photofission is a good tool, because it can reach excitation energies below those accessible by neutron-induced fission.

ACKNOWLEDGEMENTS

E.D.D. thanks the Institute of Nuclear Theory and the organizers of the INT program INT-17-1a ("Towards Predictive Theories of Nuclear Reactions Across the Isotopic Chart")

for their hospitality. E.D.D. was supported in part by the U.S. Department of Energy under Grant No. DE-FG02-97ER41042. Work at Brookhaven National Laboratory was sponsored by the Office of Nuclear Physics, Office of Science of the U.S. Department of Energy under Contract No. DE-AC02- 98CH10886 with Brookhaven Science Associates, LLC.

APPENDIX

A. Overview of experiments

In this work we focused on the three highest resolution absolute ^{235}U(n,f) cross section data sets available in the range 1–100 keV [1–3]:

- The measurement in Ref. [3] was performed at the Lawrence Radiation Laboratory (now known as LLNL) using the Livermore 100 MeV electron linac and a 200 m flight path.

- The measurements in Refs. [1] and [2] were performed at the ORELA facility at ORNL. Ref. [1] reported a conventional (n,f) measurement using a 150 m flight path. The experiment of Ref. [2] was unconventional, using a polarized neutron beam impinging on a polarized target. This permitted the determination of the spins of individual resonances. A much shorter flight path of approximately 14 m was used in Ref. [2], but the decrease in energy resolution from the reduced flight path was more than compensated by cryogenically cooling the polarized target to 0.1 K.

In all three cases, the neutrons were produced by photonuclear reactions induced by incident electron bremsstrahlung emission and then passed through a light water moderator. In each experiment, the targets were enriched in ^{235}U. Contaminants (either ^{238}U or ^{16}O for the oxide targets) were properly accounted for.

There are other experiments reporting data in the energy range of interest to us, but we found them less informative for a variety of reasons:

- The experiments of Refs. [24–28] all have inferior energy resolution. The data in Ref. [27] were actually taken as a scoping study for the experiment in Ref. [28]. There are other experiments in this energy range that have substantially worse energy resolution and are not listed in Table III.

- Ref. [32] lacks adequate published documentation.

- The uncertainty data needed for evaluation purposes was either missing or not understandable from the experiments reported in Refs. [30, 31, 34, 35]. The data in Ref. [30] were actually taken as a scoping study for the experiment in Ref. [3] used in our analysis.

- Ref. [33] was withdrawn.

- Refs. [29, 32, 36, 37] used a nuclear explosive as the neutron source and therefore have unquantifiable uncertainties in both the flight path used and the neutron fluence.

Table III summarizes these experiments. As is usual for neutron resonance measurements, the incident neutron energy in all cases was determined using time of flight (ToF).

Fröhner and Haddad [39] performed a detailed study of sources of uncertainty in ToF measurements. They argue that the uncertainty on the determined incident energy is given by $\Delta E/E = \sqrt{a + bE}$ with constants a and b. Here, a depends on overall flight path length, the neutron production target thickness and the moderator thickness surrounding the neutron production target. The constant b depends on the rescattering time in the neutron source, moderator and target (including thermally induced jitter) and the overall flight path length. In all of the experiments considered, these effects were carefully considered and we believe the reported energy resolutions for the experiments are reasonable.

Leal *et al.* [40] additionally advocate a cross section normalization factor of the form $a + b\sqrt{E}$. Given the limited energy range over which we considered cross section data, the additional $\sqrt{E}$ dependence was not found to be needed.

B. Simplified formula for $C(0)$

Equation (11) was obtained by stitching together the two expressions valid in the limits $x \gg 1$ and $x \ll 1$. The effectiveness of this approximation is illustrated by the plot of $C_{icc'}(0)$ versus $\Gamma/\bar{D}$ in Fig. 9. The approximation is poorest when the magnitude of Γ approaches that of $\bar{D}$, as is to be expected. Figure 10 contains complementary information on the extent to which the ε-dependence of $C_{icc'}(\varepsilon)$ is reproduced when the approximation to $C_{icc'}(0)$ is good.

Ref.	Pub. Year	Author	EXFOR (sub)Entry	Facility/Laboratory	Flight Path	Energy resolution (keV)
[3]	1971	C. D. Bowman *et al.*	10419.002	LRL (now LLNL) Electron Linac	250 m	0.010-0.007
[1]	1974	R. B. Perez *et al.*	10302.002	ORELA, ORNL	151.9 ± 0.1 m	0.025
[2]	1978	M. S. Moore *et al.*	10629.004	ORELA, ORNL	13.40 m[a], 15.28 m[b]	0.00005
[35]	1965	Wang *et al.*	40271.003	JINR, Dubna	1000 m	0.05
[36]	1966	R. D. Albert	12343.002	AGT, LRL (now LLNL)	1280 km	0.10
[32]	1966	W. K. Brown *et al.*	12432.002	UGT, LASL (now LANL)	Unknown	0.033
[28]	1970	B. H. Patrick *et al.*	20461.002	Harwell 45 MeV Linac	97.5 m	0.18
[29]	1970	J. D. Cramer	10057.004	UGT, LASL (now LANL)	214.43 m	0.1
[30]	1970	C. D. Bowman *et al.*	10170.002, .003	LRL (now LLNL) Electron Linac	250 m	0.05-0.1
[37]	1971	J. R. Lemley *et al.*	10120.002	UGT, LASL (now LANL)	Unclear[c]	0.004
[24]	1971	J. Blons *et al.*	20483.002	60 MeV Saclay LINAC	50.07 m	≈ 0.9
[27]	1972	D. B. Gayther *et al.*	20422.002	Harwell 45 MeV Linac	97.5 m	0.25
[31]	1975	E. Migneco *et al.*	20783.002	CBNM Linear Accelerator, Geel	60.58 m	0.0007
[33]	1976	R. Gwin *et al.*	10267.024	ORELA, ORNL	40 m	0.009
[34]	1976	C. Wagemans, A. J. Deruytter	20826.004	CBNM Linear Accelerator, Geel	30 m	0.025
[25]	1980	T. A. Mostovaya *et al.*	40616.004	Electron Linear Accelerator 'FAKEL', Kiev	26 cm	0.06
[26]	1984	L. W. Weston, J. H. Todd	12877.004	ORELA, ORNL	20 m	0.10

[a] Fssion monitor

[b] Transmission monitor

[c] Only distance to borehole given

TABLE III. Absolute ^{235}U(n,f) cross section measurements in the range 10–25 keV, retrieved from the EXFOR library [38]. Only the first three measurements, above the line in the table, are used in the present analysis. See text for details.

Errors in the approximation of $C_{ic\neq c'}(\varepsilon)$ by Eq. (10) can be sizeable ($\approx 100\%$), but only when it is an order of magnitude smaller than $C_{icc}(\varepsilon)$. The approximation of $C_{icc}(\varepsilon)$ is, by contrast, always reasonable, the percentage error being never more than 10% (even when $\Gamma \approx \bar{D}$). For the reaction studied here, there are only a few fission channels and C_{icc} term should dominate. Thus, Eq. (10) should suffice to approximate a calculation of $C(\varepsilon)$ based on Eq. (9) to within an error of 10% or so.

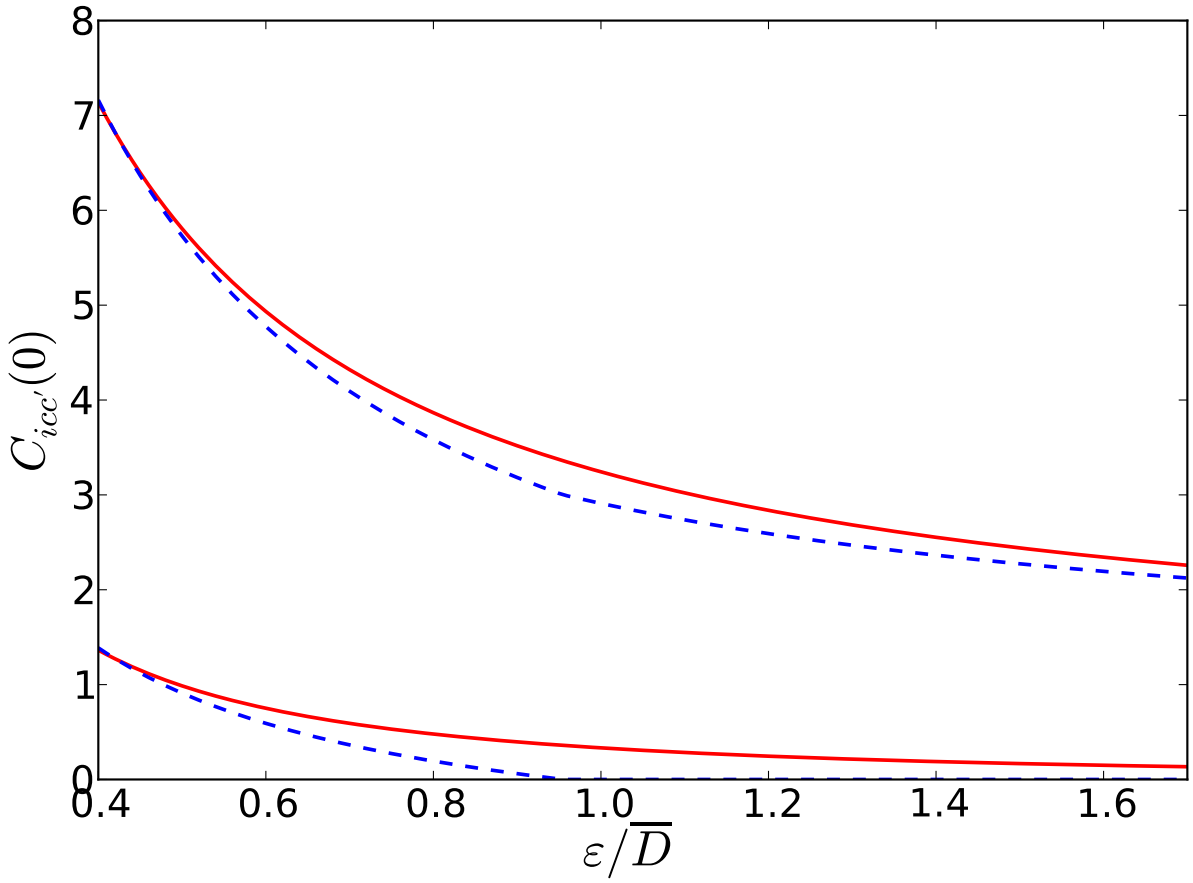

FIG. 9. Plot of $C_{icc'}(0)$ versus $\Gamma/\bar{D}$ (≥ 0.4). Upper and lower curves are for $c = c'$ and $c \neq c'$, respectively. Solid lines: evaluation of Eq. (9). Dashed lines: approximation in Eq. (10).

C. Effect of finite energy resolution

Under the assumption that cross sections are reported as averages over energy bins of fixed width ΔE, $R(\varepsilon)$ in Eq. (12) is replaced by

$$R(\varepsilon, \Delta E) = R(0)\, L\big(\tfrac{\varepsilon}{\Gamma}, \tfrac{\Delta E}{\Gamma}\big)\,, \tag{16}$$

where [22]

$$\begin{aligned} L(y,z) = \frac{1}{z^2}\Bigg[&(y+z)\arctan(y+z) + (y-z)\arctan(y-z) - 2y\arctan(y) \\ &- \tfrac{1}{2}\ln\frac{1+(y+z)^2}{1+y^2} - \tfrac{1}{2}\ln\frac{1+(y-z)^2}{1+y^2}\Bigg]. \end{aligned} \tag{17}$$

With a view to establishing the properties of $L(y,z)$, it is helpful to study $L(0,z)$ and $l(y,z) = L(y,z)/L(0,z)$ separately. As noted by Gibbs [22], a simple approximation of $L(0,z)$ is viable (see Fig. 11), namely,

$$L(0,z) \approx \frac{1}{1+z/\pi}. \tag{18}$$

The qualitative character of $l(y,z)$ depends on the magnitude of z. It is the behavior for small and large z, which is of interest to us. For $z < \frac{1}{2}$, $l(y,z) \approx (1+y^2)^{-1}$, i.e., as one would expect for good energy resolution, the dependence on ε is essentially unchanged from that in Eq. (12). For $z \gg 1$, the variable $\rho = y/z$ is preferred to y (appropriate for $z \lesssim 1$); in terms of physical parameters, this amounts to relating $R(\varepsilon, \Delta E)$ to $\varepsilon/\Delta E$ and $\Delta E/\Gamma$,

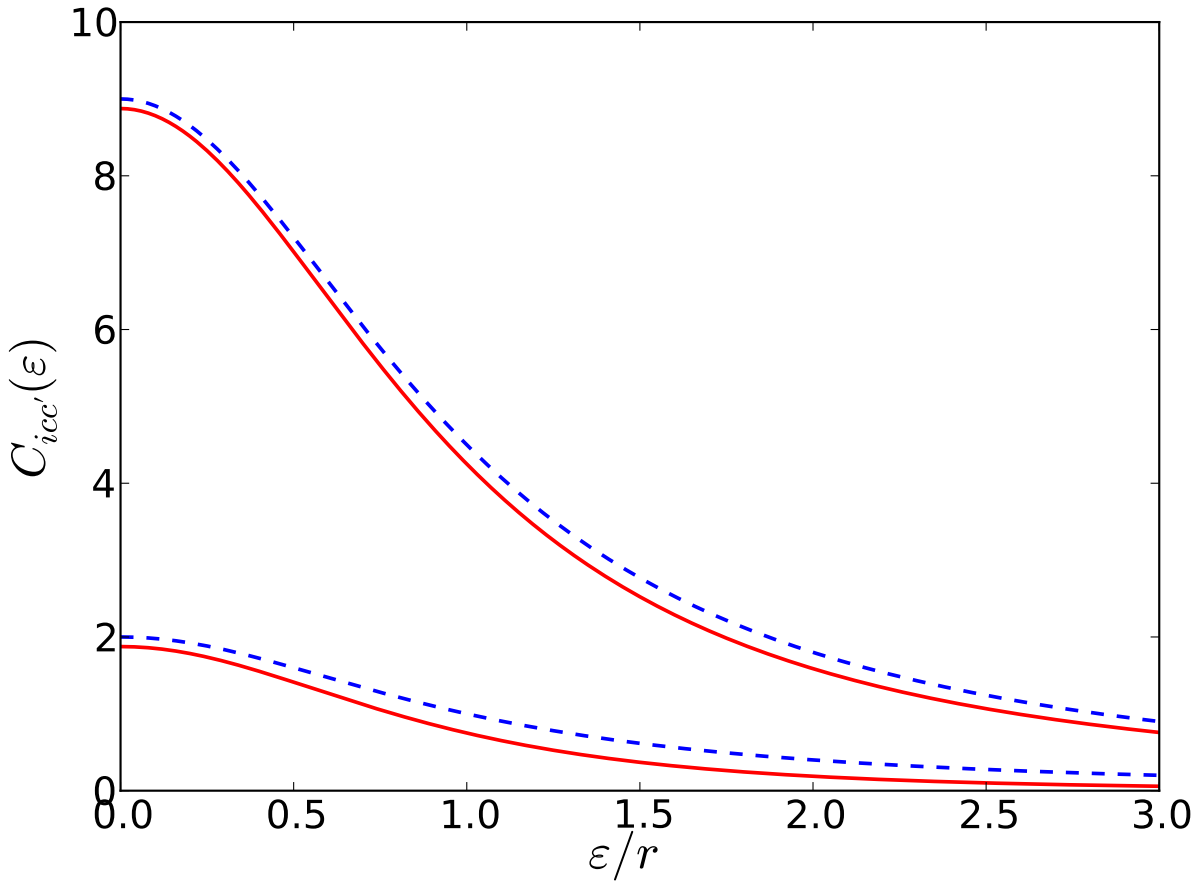

FIG. 10. Plot of $C_{icc'}(\varepsilon)$ versus ε/Γ for $x = 1$ (a value of x appropriate to the resolved resonance regime of ^{235}U). Upper and lower curves are for $c = c'$ and $c \neq c'$, respectively. Solid lines: evaluation of Eq. (9). Dashed lines: approximation in Eq. (10).

not ε/Γ and $\Delta E/\Gamma$.

The limit

$$\lim_{z\to\infty} l(\rho z, z) = (1-|\rho|)\Theta(1-|\rho|) \qquad (\rho \text{ fixed}) \tag{19}$$

forms the basis for an approximate representation of $R(\varepsilon, \Delta E)$. Figure 12 demonstrates how rapidly this limit is attained. Combining our results on $L(y, z)$, we obtain Eq. (15).

D. Realistic Modeling

Here we provide details of the Mazama model used to compute the cross section shown in Fig. 4 and the autocorrelation parameters listed in Table I. The model is defined by a matrix Hamiltonian acting in a space comprising the entrance channel wave function on a

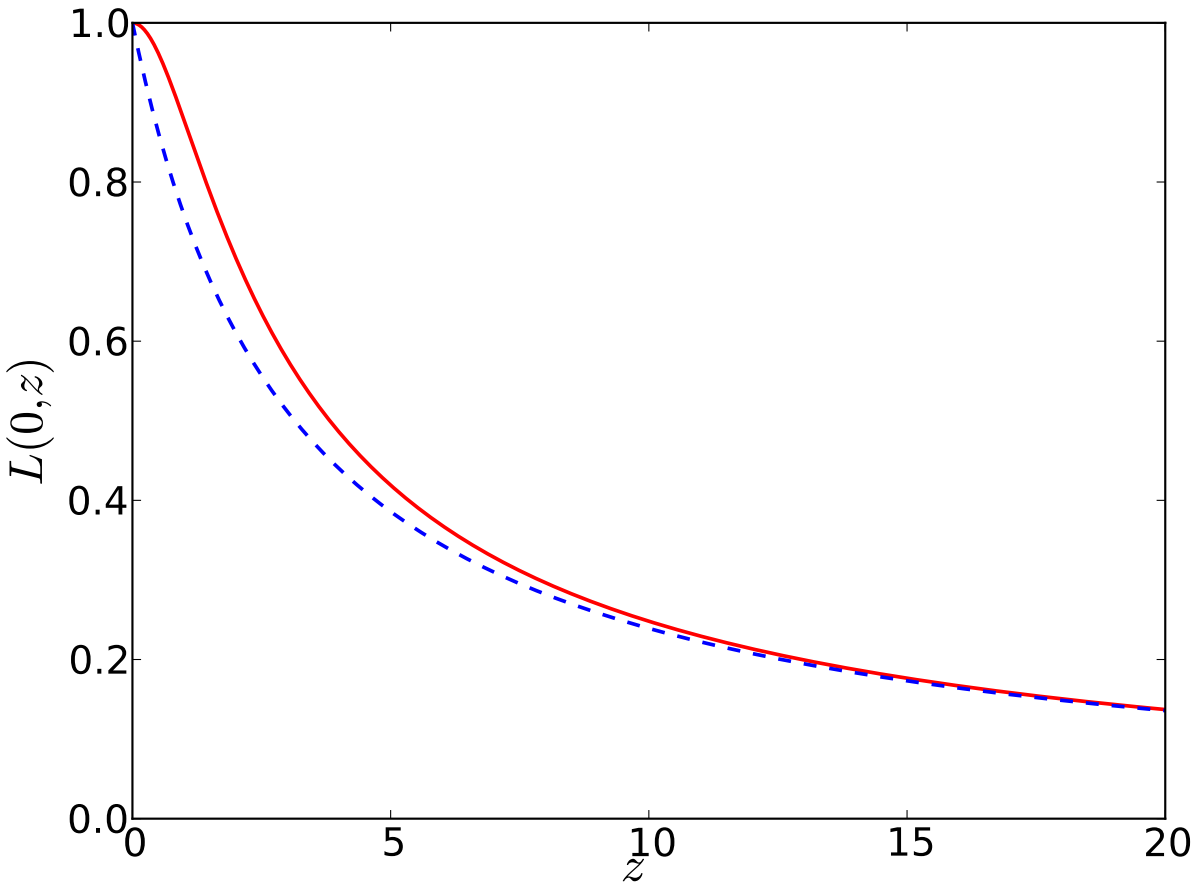

FIG. 11. Plot of $L(0, z) = [2z\arctan(z) - \ln(1+z^2)]/z^2$ versus z. Solid line: exact evaluation of $L(0, z)$. Dashed line: approximation in Eq. (18).

coordinate-space mesh r_i and one or more sets of internal states. Compound nucleus states are identified with GOE Hamiltonian eigenstates. To the real GOE resonance energies are added fixed imaginary energies associated with the gamma decay widths. In addition, the Hamiltonian includes coupling to one or more fission channels, represented as discrete doorway states that couple to the compound nucleus states. The inelastic S-matrix elements are found from solving a Schrödinger equation with a boundary condition on the entrance-channel wave function.

The key physical parameters are:

- the Woods-Saxon potential in the entrance channel sector characterized by the usual parameters $(V_{ws}, a_0, R_0 = r_0 A^{1/3})$;

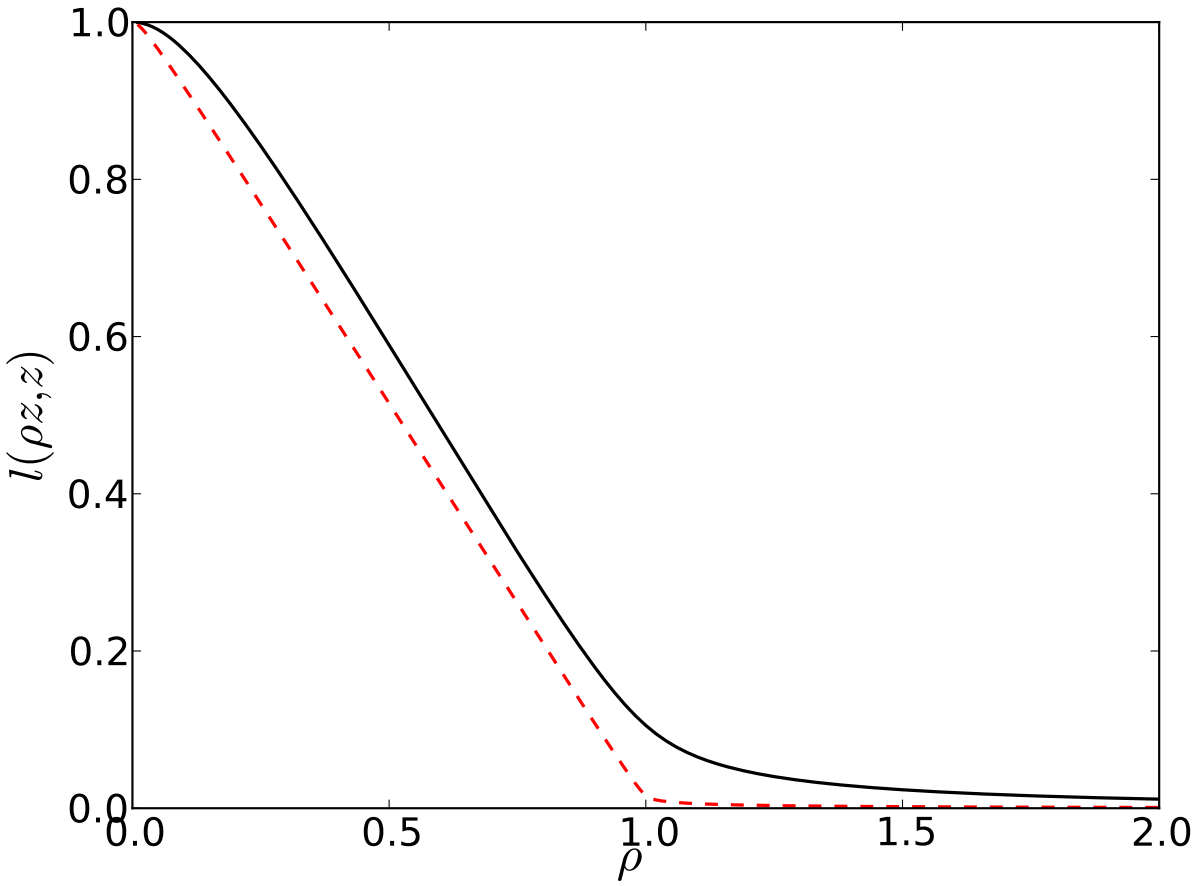

FIG. 12. Plot of $l(\rho z, z)$ versus $\rho = \varepsilon/\Delta E$ for two choices of $z = \Delta E/\Gamma$: $z = 10$ (solid line), and $z = 100$ dashed line.

- the average level spacing $\bar{D}$ of the compound-nucleus states populated from an entrance channel;

- the gamma decay width of the compound-nucleus states, assumed to be the same for all states;

- the number of the fission doorway states (each representing a fission channel) and their fission decay widths;

- the Porter-Thomas distributed coupling matrix elements between the entrance channel and the compound-nucleus states;

- the Porter-Thomas distributed coupling matrix elements between the compound-nucleus states and the fission doorway states.

For the calculations reported here, the Woods-Saxon parameters are close to those obtained by a global fit of single-particle properties at the Fermi surface [23]. The level spacing D and Γ_γ are the same as in Table I. The coupling matrix elements between the compound-nucleus states $|\mu\rangle$ and the entrance channel $|n\rangle$ are parameterized as

$$\langle n, i|v\ \mu\rangle = v_n s_\mu, \tag{20}$$

where i is a mesh point close to the nuclear surface and s_μ is a Gaussian random variable of unit variance. The strength v_n is fitted to the integrated inelastic cross section over the energy interval 10–100 eV.

There is considerable ambiguity in choosing the parameters associated with the fission channels. In this work we assume that there are 3 fission channels, each coupled to the compound nucleus states with matrix element $\langle\mu|v|f\rangle = v_f s_\mu$. The strength v_f is chosen to make the average mixing between the fission channels and the compound states uniform. In effect, the fission channels are part of the GOE, but with different decay widths. This leaves a single parameter to be determined, namely the decay width of the fission channels. We determine it by fitting to α^{-1} from Table I. The values of the parameters are given in Table II.

parameter	value
resonance spacing	$D = 0.94$ eV
capture width	$\bar{\Gamma}_\gamma = 0.038$ eV
Woods-Saxon well	$V_0 = 44$ MeV
”	$a_0 = 0.65$ fm
”	$r_0 = 1.25$ fm
n-c coupling	$v_n = 2.2$ keV
c-f coupling	$v_f = 5.1$ eV
fission width, per channel	$\bar{\Gamma}_f = 0.040$ eV
no. of fission channels	$N_f = 3$
mesh spacing	$\Delta r = 0.5$ fm

TABLE IV. Hamiltonian parameters for simulating neutron reactions on ^{235}U with the Mazama code. All parameters except v_n are insensitive to the mesh spacing of the entrance channel.

[1] R. B. Perez, G. de Saussure, E. G. Silver, R. W. Ingle, and H. Weaver, Nucl. Sci. Eng. **55**, 203 (1974).

[2] M. S. Moore, J. D. Moses, G. A. Keyworth, J. W. T. Dabbs, and N. W. Hill, Phys. Rev. C **18**, 1328 (1978).

[3] C. D. Bowman, G. S. Sidhu, M. L. Stelts, and J. C. Browne, in Proceedings of the Third Conference on Neutron Cross Sections and Technology, Knoxville, 1971, USAEC report CONF-710301, Vol. II, p. 584.

[4] B. W. Allardyce, W. R. Graham, and I. Hall, Nucl. Phys. **52**, 239 (1964).

[5] I. Hall, Phys. Lett. **10**, 199 (1964).

[6] T. Ericson, Phys. Rev. Lett. **5**, 430 (1960).

[7] T. Ericson, Ann. Phys. (N.Y.) **23**, 390 (1963).

[8] A. Richter, in ”Nuclear Spectroscopy and Reactions, Part B”, ed. J. Cerny, (Academic Press, 1974).

[9] D. Brink and R. Stephen, Phys. Lett. **5** 77 (1963).

[10] P. Bizzeti and P. Maurenzig, Il Nuovo Cimento **47** 29 (1967).

[11] J. Ramos, et al., Phys. Rev. Lett. **107** 176807 (2011).

[12] B. Dietz, A. Richter and R. Samajdar, Phys. Rev. E **92** 022904 (2015).

[13] F. J. Dyson, J. Math. Phys. **3**, 166 (1962).

[14] T. E. O. Ericson, B. Dietz, and A. Richter, Phys. Rev. E **94**, 042207 (2016).

[15] J. Bondorf and R. B. Leachman, Kgl. Danske Videnskab. Selskab, Mat. Fys. Medd. **34**, No. 10 (1965).

[16] W. R. Gibbs, Phys. Rev. **153**, 1206 (1967).

[17] R. Capote *et al.*, Nucl. Data Sheets **148**, 254 (2018). See also R. Capote *et al.*, *ibid.* **110**, 3107 (2009).

[18] D. A. Brown *et al.*, Nucl. Data Sheets **148**, 1 (2018).

[19] A. D. Carlson *et al.*, Nucl. Data Sheets **148**, 143 (2018).

[20] See Supplemental Material at [URL will be inserted by publisher] for the programs, scripts and data used to produce Figs. 2-6 and Table I.

[21] ENDF-VIII.0 evaluated cross sections, National Nuclear Data Center (http://www.nndc.bnl.gov).

[22] W. R. Gibbs, Phys. Rev. **139**, B1185 (1965); W. R. Gibbs, Los Alamos Scientific Laboratory Report LA-3266, 1965 (unpublished).

[23] A. Bohr and B. R. Mottelson, *Nuclear Structure* (W. A. Benjamin, New York, 1969), Vol. I.

[24] J. Blons, Nucl. Sci. Eng. **51**, 130 (1973).

[25] T. A. Mostovaya, V. I. Mostovoy, S. A. Biryukov, A. A. Osochnikov, and A. V. Tsvestkov, in Proceedings of the Fifth All-Union Conference on Neutron Physics, Kiev, 1980, Vol. 3, p. 30 (in Russian).

[26] L. W. Weston and J. H. Todd, Nucl. Sci. Eng. **88**, 567 (1984).

[27] D. B. Gayther, D. A. Boyce, and J. B. Brisland, in *Neutron Standard Reference Data*, proceedings of the Second IAEA Panel on Neutron Standard Reference Data, Vienna, 1972 (IAEA, Vienna, 1974), p. 201.

[28] B. H. Patrick, M. G. Sowerby, and M. G. Schomberg, J. Nucl. Energy **24**, 269 (1970).

[29] J. D. Cramer, Los Alamos Scientific Laboratory Report LA-4420, 1970 (unpublished).

[30] C. D. Bowman, M. L. Stelts, and R. J. Baglan, Lawrence Radiation Laboratory Report UCRL-72472, 1970 (unpublished).

[31] M. G. Cao, E. Migneco, J. P. Theobald, J. A. Wartena, and J. Winter, J. Nucl. Energy **22**, 211 (1968); G. Lanzanó, and E. Migneco, Nuov. Cim. A **41**, 259 (1977); E. Migneco, P. Bonsignore, G. Lanzanó, J. A. Wartena, and H. Weigmann, in *Nuclear Cross Sections and Technology*, proceedings of Conference on Nuclear Cross Sections and Technology, Washington, DC, 1975, edited by R. A. Schrack and C. D. Bowman (NBS, Washington, DC, 1975), NBS Spec. Publ. 425, Vol. 2, p. 607.

[32] W. K. Brown, D. W. Bergen, and J. D. Cramer, in Proceedings of Conference on Neutron Cross Section Technology, Washington, DC, 1966, edited by P. B. Hemmig, USAEC report CONF-660303, Book 2, p. 971.

[33] R. Gwin, E. G. Silver, R. W. Ingle, and H. Weaver, Nucl. Sci. Eng. **59**, 79 (1976); R. Gwin, R. R. Spencer, R. W. Ingle, J. H. Todd, and S. W. Scoles, *ibid.* **88**, 37 (1984).

[34] C. Wagemans and A. J. Deruytter, Ann. Nucl. Energy **3**, 437 (1976).

[35] Wang Shih-Ti, Wang Yung-Cháng, E. Dermendzhiev, and Yu. V. Ryabov, Sov. J. At. Energy **19**, 43 (1965).

[36] R. D. Albert, Phys. Rev. **142**, 778 (1968).

[37] J. R. Lemley, G. A. Keyworth, and B. C. Diven Nucl. Sci. Eng. **43**, 281 (1971).

[38] N. Otuka, E. Dupont, V. Semkova *et al.*, Nucl. Data Sheets **120**, 272 (2014).

[39] F. H. Fröhner and E. Haddad, Nucl. Phys. **71**, 129 (1965).

[40] L. C. Leal, H. Derrien, N. M. Larson, and R. Q. Wright, Nucl. Sci. Eng. **131**, 230 (1999).